

pubs.acs.org/jcim Article

Transition Path Sampling Study of Engineered Enzymes That Catalyze the Morita-Baylis-Hillman Reaction: Why Is Enzyme Design so Difficult?

Sree Ganesh Balasubramani, Kseniia Korchagina, and Steven Schwartz*



Cite This: J. Chem. Inf. Model. 2024, 64, 2101–2111



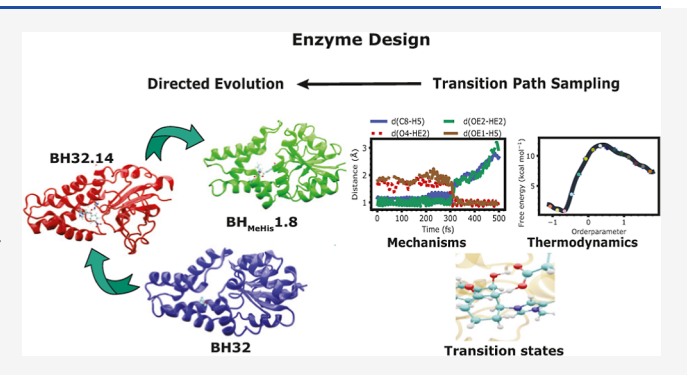
ACCESS I

Metrics & More

Article Recommendations

Supporting Information

ABSTRACT: It is hoped that artificial enzymes designed in laboratories can be efficient alternatives to chemical catalysts that have been used to synthesize organic molecules. However, the design of artificial enzymes is challenging and requires a detailed molecular-level analysis to understand the mechanism they promote in order to design efficient variants. In this study, we computationally investigate the mechanism of proficient Morita—Baylis—Hillman enzymes developed using a combination of computational design and directed evolution. The powerful transition path sampling method coupled with in-depth post-processing analysis has been successfully used to elucidate the different chemical pathways, transition states, protein dynamics,



and free energy barriers of reactions catalyzed by such laboratory-optimized enzymes. This research provides an explanation for how different chemical modifications in an enzyme affect its catalytic activity in ways that are not predictable by static design algorithms.

■ INTRODUCTION

Naturally occurring enzymes are evolved to catalyze various chemical reactions of biological importance with enhanced rates compared to the corresponding uncatalyzed reactions. 1-3 However, natural enzymes cannot catalyze many chemical reactions of relevance in organic synthesis and industrial applications. 4,5 In this case, the strategy of computational design followed by directed evolution of proteins is applicable. 6,7 Evolution often results in proteins with catalytic mechanisms that are distinct from those present in the original design model, highlighting the complexities of predicting and designing optimal active site arrangements for performing new chemistries. 8,9

One of the important organic transformations catalyzed only by synthetic proteins is the Morita–Baylis–Hillman (MBH) reaction. This reaction is useful for C–C bond formation between an activated alkene and a carbon electrophile promoted by small nucleophilic catalysts such as DABCO (triethylenediamine), DMAP(4-dimethylaminopyridine), DBU (diazabicycloundecene), and imidazole. However, the use of these catalysts results in very low conversions (<0.5% after 22 h). Designing enzymes that can catalyze MBH-type reactions can be quite useful for the organic synthesis of natural products.

Bjelic et al. used the Rosetta¹⁸ software to computationally design 48 proteins which contain active sites that were predicted to catalyze a MBH reaction, out of which two variants showed catalytic activity.¹⁷ One particular variant

called BH32 [Protein Data Bank (PDB) ID: 3U26] showed modest catalytic activity and was crystallized. With the BH32 variant as the starting point, Crawshaw et al. used a combination of computational design and directed evolution to obtain an efficient and enantioselective enzyme (BH32.14) that catalyzes the same MBH reaction. 16 The BH32.14 variant exhibited very high conversion (>80% after 22 h). This protein takes 2-cyclohexen-1-one and 4-nitrobenzaldehyde as substrates and catalyzes the formation of 2-[hydroxy(4nitrophenyl)methyl]cyclohex-2-en-1-one. To understand the mechanism promoted by this protein, Crawshaw et al. performed computational analysis of this system by building a density functional theory (DFT) cluster model. They picked 273 atoms from the active site of the crystallized BH32.12 variant (PDB ID: 6Z1L) and docked the substrates and a water molecule as part of their model. They reported a mechanism that involved a histidine residue (His23) acting as a nucleophile, an arginine residue (Arg124) playing a key role in stabilizing some of the intermediates, and a rate-limiting chemical step that involved two proton transfers between the substrate and a water molecule. Although these theoretical

Received: January 10, 2024 Revised: February 23, 2024 Accepted: February 26, 2024 Published: March 7, 2024





Figure 1. Chemical scheme for the proposed mechanism depicting the steps involved in the MBH reaction between 2-cyclohexen-1-one (1) and 4-nitrobenzaldehyde (2) leading to the formation of 2-[hydroxy(4-nitrophenyl)methyl]cyclohex-2-en-1-one (3) catalyzed by a nucleophile $(\ddot{N}uc)$ and a water molecule. The atoms labeled in red are directly involved in the proton transfer between the water molecule and the intermediate 2 and are given unique names to label them for the computational analysis in this manuscript.

cluster model studies have been highly helpful in understanding electronic structures and suggesting reaction mechanisms, the dynamics of these systems has not been investigated. The approach is restricted to the analysis of chemical structure snapshots. Therefore, the use of dynamics techniques could offer new insights into the ways in which different protein mutations affect their ability to function.

Further studies by Crossley et al. showed that a greater increase in the catalytic activity of this protein can be achieved by replacing the His23 residue with a non-canonical amino acid MeHis (N_{δ} -methylhistidine). This mutation followed by directed evolution resulted in the $BH_{MeHis}1.8$ enzyme that is an order of magnitude more active than the BH32.14 enzyme. Significantly altered catalytic mechanisms were suggested for this enzyme because the Arg124 residue was selected out of the structure in favor of a glutamic acid residue (Glu26). Apart from a water-mediated reaction mechanism, depending on the protonation state of Glu26, there is a possibility of direct proton transfers between the substrates and Glu26. Crossley et al. also created mutations of the BH_{MeHis}1.8 enzyme by replacing the Glu26 with a glutamine residue to understand its role in catalysis and observed a 20-fold reduction in reaction rates. From these studies, it is evident that small changes to the protein alter its catalytic activity significantly, and so further investigation is required to understand the exact mechanistic details of this enzyme-catalyzed reaction.

In this article, we employ molecular dynamics (MD) simulations with quantum mechanics/molecular mechanics (QM/MM) potentials and the transition path sampling (TPS) method^{20,21} to elucidate the mechanisms of the MBH reaction catalyzed by several variants of this enzyme. TPS has proven to be a powerful tool to characterize enzyme-catalyzed reactions and has been extensively employed to calculate their transition states, reaction coordinates, and free energies.^{22–26} The mechanisms that we investigated include the water-mediated proton transfers promoted by the BH32.14 variant and four different pathways promoted by the BH_{MeHis}1.8 enzyme, three of which involve a water-mediated mechanism, while the fourth is a direct proton transfer mediated by the GluH26 residue. By analyzing the trajectories in the TPS ensemble to calculate the transition states and free energies, we find that the

most efficient mechanism involves the direct transfer of the two protons between the substrate and the enzyme.

COMPUTATIONAL METHODS

The BH32.12 and BH $_{\rm MeHis}$ 1.8 enzymes take in 2-cyclohexen-1-one and 4-nitrobenzaldehyde as substrates (see Figure 1) and lead to the formation of 2-[hydroxy(4-nitrophenyl)methyl]-cyclohex-2-en-1-one. The rate-determining step is the conversion of intermediate 2 to intermediate 3, which involves the transfer of two protons between the substrate and either a water molecule or an enzyme variant with a suitable residue.

The computational study of each system was carried out in three steps. First, the crystal structures of BH32.12 and $\rm BH_{MeHis}1.8$ are modified by changing the substrates with which they were crystallized at the active site to intermediate 2 and using the His23 residue and the MeHis23 residue as nucleophiles, respectively. This was followed by solvating, heating, and equilibrating the enzymatic systems. The second step involves sampling TPS trajectories connecting the reactant (intermediate 2) and product (intermediate 3) states. The final step involves using the TPS trajectories to perform committor analysis and window-based sampling to calculate transition states and free energies, respectively.

System Preparation. The MBH reaction mechanisms are studied using hybrid QM/MM^{27,28} based TPS simulations. The CHARMM force field²⁹ is used for describing forces on the atoms in the MM partition, whereas the semiempirical PM3³⁰ method is used for the atoms in the QM partition. The QM and MM partitions are coupled using the generalized hybrid orbital (GHO) scheme.³¹

After partitioning the enzymatic systems into QM and MM regions, they were solvated with TIP3P water molecules³² in a nanodroplet sphere with the dimension fixed at 15 Å away from the protein's surface, and the total charge was neutralized using potassium ions. The solvated enzymes are minimized with 1000 steps of the steepest descent method, followed by 10,000 steps of the adopted basis Newton–Raphson method.

After minimization, the enzymatic systems were slowly heated to 300 K for 35 ps. This process starts with the application of harmonic constraints on all of the atoms except on the H atoms and the TIP3P water molecules, and the

Figure 2. Proposed mechanism of the MBH reaction catalyzed by the BH32.12 enzyme. The substrate is covalently bound to the His23 residue, and oxyanionic intermediate states are stabilized by the Arg124 residue, which is essential for catalysis. The proton transfers are mediated by a water molecule.

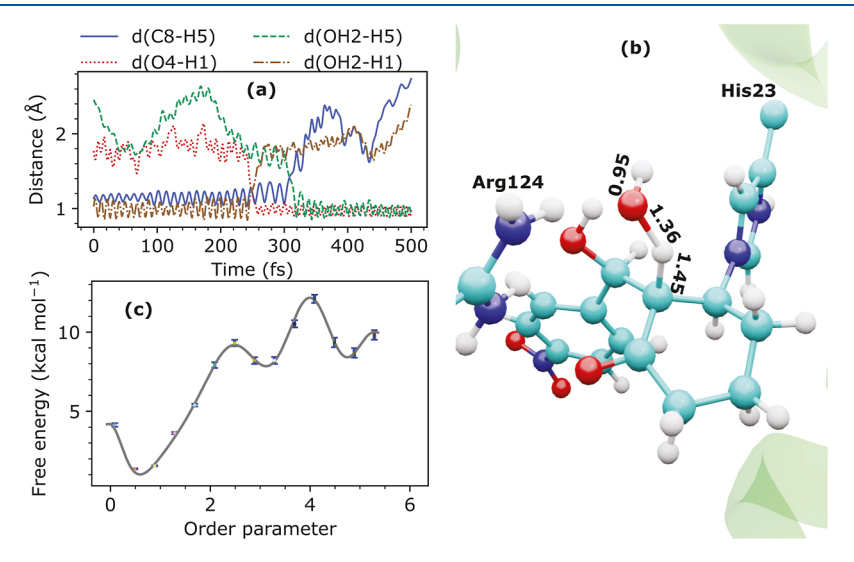


Figure 3. (a) Time series of the evolution of various proton transfer atomic distances along a typical TPS trajectory for the BH32.12 enzyme with an arginine residue and water-mediated reaction mechanism. (b) Geometry of the substrate along with the Arg124 and His23 residues at the second transition state calculated using committor analysis for a typical TPS trajectory, which indicates the formation of an OH⁻ ion. (c) Reaction free energy as a function of the order parameter $\chi = d(OH2-H1) - d(H1-O4) + d(O4-C7) + d(C7-C8) + d(C8-H5) - d(H5-OH2)$ calculated using a window-based modified TPS algorithm, where the error bars obtained from bootstrapping analysis are indicated in blue.

restraint forces are gradually reduced. After this, the systems were equilibrated for 15 ps with harmonic restraint forces, followed by equilibration for 200 ps without any constraints. During all of the MD simulations, bonds that connect hydrogen atoms in the MM partition were constrained to the corresponding equilibrium bond length values using the SHAKE procedure.³³ All simulations were performed using the CHARMM MD package.³⁴

Transition Path Sampling. TPS was used to generate an ensemble of unbiased dynamical trajectories connecting the stable reactant and product states by carrying out a random walk in the space of trajectories by means of a Metropolis Monte Carlo procedure. To classify the reactant (intermediate 2) and product (intermediate 3) states for the MBH reaction, as shown in Figure 1, we used the atomic distances between the following pairs of atoms: the C8 and H5 atoms [d(C8-H5)], the O4 and H1 atoms [d(O4-H1)], the OH2 and H5 atoms [d(OH2-H5)], and the OH2 and H1 atoms [d(OH2-H1)]. Reactant states are defined by d(OH2-H1) < 1.2 Å and d(C8-H5) < 1.3 Å, while product states are defined by d(O4-H1) < 1.2 Å and d(OH2-H5) < 1.2 Å. A biased reactive trajectory connecting the reactant and product

states was obtained by applying a harmonic force with a force constant of 15 kcal/mol/Ų between the pairs of atoms listed above and running dynamics with a 1 fs time step for a total of 500 fs starting from the equilibrated structure. This biased reactive trajectory was used as the seed, along with the help of the shooting algorithm 37,38 to generate an ensemble of ~ 200 reactive TPS trajectories for each of the enzymatic systems studied here.

Postprocessing of TPS Trajectories. To track the fluctuations in the atomic geometries and charges in the enzymatic systems during the reaction, Mulliken charge calculations and interatomic distance analyses were carried out for the TPS trajectories. Committor analysis and committor distribution analysis $^{39-41}$ were employed to calculate, respectively, the structures of transition states and reaction coordinates. Free energy profiles were calculated along the order parameter ζ defined by $\zeta = d(\text{C8-H5}) - d(\text{OH2-H5})$ using a recently developed TPS-based algorithm. A more detailed list of the computational parameters that were used to run the TPS, committor analysis, and free energy calculations can be found in the Supporting Information.

RESULTS AND DISCUSSION

Mechanism Promoted by the BH32.12 Enzyme. Crawshaw et al. observed that the Arg124 residue, a hydrogen bond donor, was essential for catalytic activity of the BH32.12 enzyme. The proposed mechanism for the reaction catalyzed by the BH32.12 enzyme is presented in Figure 2, and the mechanistic details obtained from the TPS trajectories are discussed in this section.

Examination of the TPS trajectories revealed that in this system, the reaction proceeds according to a stepwise mechanism. First, a water molecule approaches the negatively charged oxyanion (the O4 atom) and acts as a proton donor. As a result, an unstable OH⁻ ion is formed. In about 60 fs, this ion acts as a proton acceptor and breaks the C-H bond (C8 atom), forming a new water molecule. Breaking the C-H bond starts the process of charge redistribution and leads to some structural changes. Pushed by the Trp10 residue, the Arg124 residue moves to maximize the electrostatic stabilization of another newly formed oxyanion (O3 atom) (Figure 2) as the charge is redistributed. We can observe that for a typical TPS trajectory, as shown in Figure 3a, the proton transfers occur within 80 fs of each other, and during that time period, a hydroxide anion (OH⁻) is formed, which is stabilized by the Arg124 residue. Committor analysis calculations result in two transition states, and Figure 3b shows the geometrical parameters for the second transition state that involves the transfer of a proton from the C8 atom to the OH⁻ anion. This structural analysis agrees well with Mulliken's charge analysis. We observe a sharp decrease in the magnitude of the charge on the O4 atom from -0.8 to -0.4 charge units in the range of 240-275 fs (Figure S1). In turn, between 300 and 330 fs, the negative charge on the C8 atom rises from -0.3 to -0.8 charge units. The Arg124 residue stabilizes these intermediate structures. It has two hydrogen atoms (HH11 and HH21) that form hydrogen bonds with an O3 atom, then with an O4 oxyanion, and then with the O3 oxyanion (Figure 2). For example, until 170 fs, the distance between the HH21 and O3 atoms increases from 3.5 to 5.4 Å, bringing the HH21 atom closer to the negatively charged O4 anion (2.6 Å). However, during protonation of the O4 atom, its charge is neutralized, whereas the charge on the O3 atom smoothly decreases (from -0.3 to -0.7 charge units). The d(HH21-O4) distance increases to 3.7 Å throughout this time, while the d(HH21-O3) distance falls from 5.4 to 3.9 Å. Thus, during the reaction, it is clear that arginine stabilizes the oxygen atom with the highest negative charge, and these changes are accomplished by directed protein motion. Such motion is likely a reason that laboratory-evolved enzymes show greater proficiency than the initial static designs. This is a trend we have seen previously in laboratory-designed enzymes. 43,44

At the next stage of our theoretical study, the catalytic activity was assessed using free energy calculations. To carry out free energy calculations, we took into account the stepwise mechanism of this process. Two methods were taken into consideration when choosing the order parameter. The first scenario involves performing two independent free energy calculations, each with an order parameter that corresponds to the appropriate step of the reaction. The distance difference $\chi 1 = [d(O4-H1) - d(OH2-H1)]$ and the distance difference $\chi 2 = [d(C8-H5) - d(OH2-H5)]$ describes the proton transfers for the first and second steps, respectively. In both cases, we obtained a free energy value of 7 kcal/mol (Figures S2 and S3

in the Supporting Information). However, the main drawback of this approach is that we do not take into account the fact that the two proton transfers are coupled. A two-dimensional scan to calculate the free energy would be ideal in this case, but it is computationally expensive using the algorithm that is employed here. The selection of the appropriate order parameter that will sufficiently distinguish the different stable states of the biochemical process is not a trivial task. It is sometimes required to carefully consider the combination of different system parameters. 45 For this reason, we have examined an alternative approximate approach in which we define an order parameter that captures changes to both of the proton transfer bond parameters in a linear fashion. A possible linear combination of atomic distances that captures the appropriate changes is the new order parameter χ , defined by d(OH2-H1) - d(H1-O4) + d(O4-C7) + d(C7-C8) +d(C8-H5) - d(H5-OH2). The order parameter spans the range [0.0 Å, 6.0 Å] for a randomly selected trajectory from the TPS ensemble, which is divided into 15 overlapping windows. The shooting algorithm is used to harvest ~2000 short TPS trajectories within each window. Calculating the free energy (ΔG) along this order parameter (χ) via Boltzmann inversion yields two barriers that correspond to two different transition states separated by an intermediate (Figure 3c).

The intermediate state corresponds to the formation of an OH anion that is stabilized by Arg124 which is a hydrogen bond donor. The magnitude of the first barrier is 7 kcal/mol, while the magnitude of the second barrier is 10 kcal/mol. Since the intermediate has a higher value of ΔG than the reactant state and because the free energy barrier for the reverse reaction of going from the intermediate to the reactant state is only ~2 kcal/mol, it is expected that the observed overall rate of reaction is smaller because of this competing pathway. This low energy barrier (in comparison to the systems that will be addressed further) can also be explained by the fact that we do not account for the mobility of the water molecule, and this might produce an entropic contribution to the actual free energy barrier. As we describe in the conclusions section, such an effect would require TPS trajectories long enough to include diffusive water motion, and this is simply not possible in a QM/MM framework. Nevertheless, this reaction is the most efficient variant reported by Crawshaw et al. 16 from the first round of directed evolution studies, and it is much more catalytically active than the original BH32 enzyme designed by Bjelic et al. 17 A possible roadblock in quantitative comparisons between calculated and experimental kinetic parameters is that the experiments measured the steady-state kinetics (Michaelis-Menten plot), which include important factors such as protein conformational changes and substrate release, whereas our calculations were focused on the dominant ratedetermining chemical step in the reaction.

Mechanisms Promoted by the BH_{MeHis}1.8 Variants. For the BH_{MeHis}1.8 mutation, a Glu26 residue was found to play a key role in catalysis. It was observed from ProPka calculations that Glu26 had an unusually high p K_a of 8.1. Therefore, we studied several protonation states of this system, namely, (i) intermediate 2, a water molecule, and a glutamate residue, (ii) protonated intermediate 2 (at the O4 oxyanion), a water molecule, and a glutamate residue, and (iii) intermediate 2 and glutamic acid. Furthermore, to understand the role of Glu26 in the reaction mechanism, we mutated the Glu26 to a glutamine residue (Gln26) and computationally analyzed the reaction mechanism of the resulting enzyme.

Figure 4. Predicted reaction scheme for the $BH_{MeHis}1.8$ variant containing (a) the ionized form of the Glu26 residue (glutamate) on the left and (b) the glutamine Gln26 residue on the right. For the Gln26 case, the carbonyl group acts as a hydrogen bond acceptor, whereas for the glutamate case, both the OE1 and OE2 atoms with delocalized negative charge act as hydrogen bond acceptors.

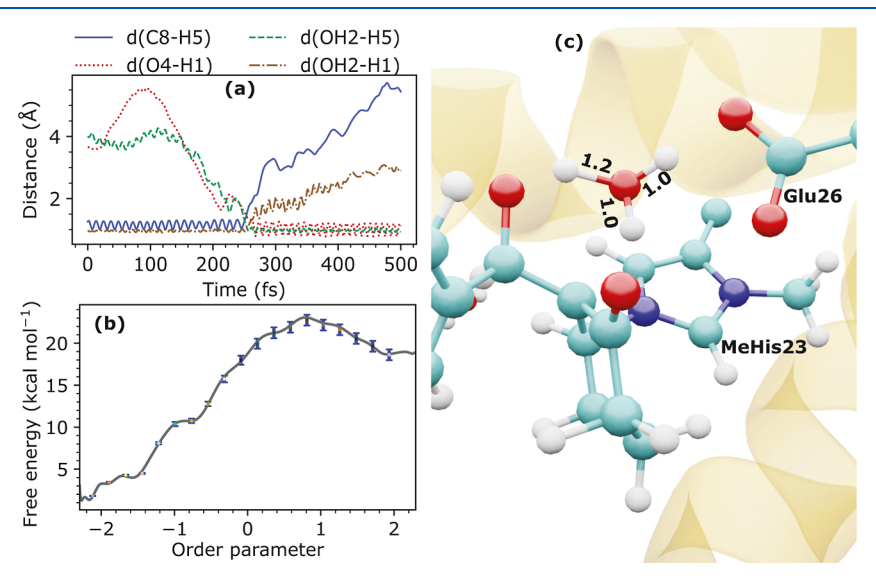


Figure 5. (a) Time series of the evolution of various proton transfer atomic distances along a typical TPS trajectory for the BH_{MeHis}1.8 enzyme with a glutamate residue and water-mediated reaction mechanism. (b) Geometry of the substrate along with the Glu26 and MeHis23 residues at the transition state calculated using committor analysis for a typical TPS trajectory, which indicates the formation of a H₃O⁺ ion. (c) Reaction free energy as a function of the order parameter $\zeta = d(C8-H5) - d(OH2-H5)$ calculated using a window-based modified TPS algorithm, where the error bars obtained from bootstrapping analysis are indicated in blue.

Mechanism Involving the Glutamate Residue. We start by discussing the TPS simulations for the system with intermediate 2, a water molecule, and the glutamate residue, as shown in Figure 4a. A water molecule orients in a bridging fashion between two hydrogen bond acceptors in this system, the O4 oxyanion on the substrate, and the OE1/OE2 atoms from the Glu26 residue. This configuration is used as the definition for the reactant state of the TPS simulations, and the atomic distances relevant for the proton transfers (H1 and H5 atoms) along a typical TPS trajectory are shown in Figure 5a, and it can be observed that these two proton transfers occur within a time period of 10 fs. From committor analysis of the TPS trajectories, we obtain the transition state geometry for this reaction, and one of the calculated transition states is depicted in Figure 5b. The average values of some of the relevant atomic distances that were obtained for an ensemble of transition states are given by $d(OH2-H5) = 1.0 \pm 0.05 \text{ Å}$, $d(OH2-H1) = 1.15 \pm 0.09 \text{ Å}, \text{ and } d(OH2-H2) = 0.97 \pm 0.09 \text{ Å}$ 0.02 Å, which indicates the formation of a symmetric

hydronium ion (H_3O^+) at the transition state. These results are quite different compared to what was calculated from the TPS simulations for the BH32.12 enzyme, whose catalytic mechanism resulted in the formation of a hydroxide anion (OH^-) at the transition state, and the two proton transfers occurred with a time lag of at least 60 fs.

The free energy as a function of the order parameter $\zeta = d(\text{C8-H5}) - d(\text{OH2-H5})$ is calculated using a randomly chosen TPS trajectory from the ensemble. The order parameter spans the range [-2.2 Å, 2.2 Å] for the chosen trajectory which is divided into 15 overlapping windows. Within each window, 2500 short TPS trajectories are collected using the shooting algorithm, and the resulting free energy profile from these calculations is reported in Figure 5c. It can be observed that the free energy barrier for this reaction is ~ 20 kcal mol⁻¹. An important distinction in the free energy profile is that the BH_{MeHis}1.8 enzyme has a single broad barrier, while the BH32.12 enzyme has two barriers separated by an intermediate state, which would produce an experimentally

Figure 6. Reaction mechanism promoted by the $BH_{MeHis}1.8$ enzyme with a GluH26 residue protonating the O4 oxyanion and a catalytic water molecule involved in the transfer of proton from the substrate to the glutamate residue.

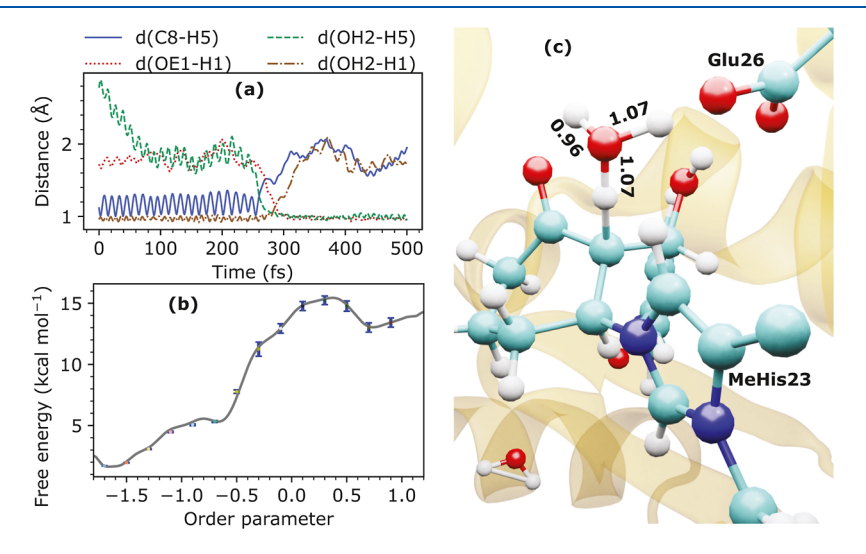


Figure 7. (a) Time series of the evolution of various proton transfer atomic distances along a typical TPS trajectory for the BH_{MeHis}1.8 enzyme with a glutamic acid residue and water-mediated reaction mechanism. (b) Geometry of the substrate along with the GluH26 and MeHis23 residues at the transition state calculated using committor analysis for a typical TPS trajectory, which indicates the formation of a H₃O⁺ ion. (c) Reaction free energy as a function of the order parameter $\zeta = d(C8-H5) - d(OH2-H5)$ calculated using a window-based modified TPS algorithm, where the error bars obtained from bootstrapping analysis are indicated in blue.

observed lower reaction rate for the latter enzyme. This is supported by the observation of Crossley et al. that the $BH_{MeHis}1.8$ is an order of magnitude more active than the older BH32.12 variant. ¹⁹

Mechanisms Involving the Glutamic Acid Residue. When the Glu26 residue exists in its nonionized glutamic acid form (called the GluH26 residue), it can directly protonate the substrate, which can result in two possible pathways for the reaction. First, we discuss the mechanism that involves a catalytic water molecule from Figure 6.

In the presence of a water molecule, during the equilibration MD simulations, it was observed that the glutamic acid is ionized, and it protonates the O4 oxyanion. Therefore, for the TPS simulations, we started with the protonated substrate, a water molecule, and the glutamate residue as the reactant state. For a typical TPS reactive trajectory, we observed the transfer of the proton from the C8 atom to the water molecule, resulting in the formation of a hydronium ion which quickly dissociates through the transfer of a proton to the glutamate residue, resulting in the formation of the product and the glutamic acid residue GluH26, which is shown in Figure 7a. Using committor analysis, we calculated the transition state geometry of this system for a typical TPS trajectory, and it is shown in Figure 7b. It can be observed that a symmetrical

 ${
m H_3O^+}$ ion is formed and is located between the substrate and the Glu26 residue. The average interatomic distances for this hydronium ion are $d({
m OH2-H1})=0.93\pm0.02$ Å, $d({
m OH2-H2})=1.06\pm0.05$ Å, and $d({
m OH2-H5})=1.11\pm0.06$ Å, which are calculated from an ensemble of transition states corresponding to various trajectories from the TPS ensemble. From Figure 7c, it can be observed that the free energy barrier for this reaction is ~14 kcal/mol. This free energy barrier is 6 kcal/mol smaller compared to the 20 kcal/mol barrier that was obtained for the system with the glutamate residue and a catalytic water molecule, as discussed in the subsection. This system also exhibits a single free energy barrier between the reactant and product states and is therefore expected to be catalytically more active than the BH32.12 variant.

When water is not involved in the proton transfers, the glutamic acid residue (GluH26) can directly protonate the O4 oxyanion and deprotonate the C8 atom of the substrate, and the chemical steps involved in this reaction are depicted in the scheme shown in Figure 8. From a typical TPS trajectory, we can detect a short temporal lag (\sim 10 fs) between the two proton transfers, as shown in the time series of relevant atomic distances in Figure 9a, and it can be described as simultaneous. The transition state calculated using committor analysis from a typical TPS trajectory is shown in Figure 9b, and it can be

Figure 8. Reaction scheme for the direct protonation mechanism between the substrate and the Glu26 residue. The atoms marked in red color are given special labels, which will be used in the analysis.

observed that the oxyanion O4 gets protonated by the GluH26 residue, while the deprotonation of the C8 atom is almost complete. This is in contrast to the previously discussed systems that involve a catalytic water molecule where the C8 deprotonation occurs first, resulting in the formation of hydronium ion that is stabilized by the Glu26 residue at the transition state. Since the formation of the $\rm H_3O^+$ intermediate as well as the catalytic water molecule are avoided, this system is expected to be catalytically more efficient among the $\rm BH_{MeHis}1.8$ systems studied in this work.

The free energy profile for this system was calculated along the order parameter $\zeta = d(\text{C8-H5}) - d(\text{OH2-H5})$, and the result is shown in Figure 9c. The barrier is calculated to be ~11 kcal/mol, which is smaller than the barrier calculated for the other two mechanisms involving the BH_{MeHis}1.8 variant discussed previously, both of which involved water-mediated proton transfers. This observation is in line with what is suggested as the most plausible mechanism by Crossley et al., ¹⁹ who proposed that in the absence of Glu26, the catalysis may proceed through the less efficient water-mediated proton transfer, similar to the mechanism proposed for the BH32.14 variant. ¹⁶ We further add to their point that, depending on the protonation state of the Glu26 residue, the water-mediated

mechanism is a possible pathway, albeit with a larger free energy barrier.

Mechanism of the Glutamine Variant. The reaction mechanism for the Gln26 mutation of the BH_{MeHis}1.8 variant is shown in Figure 4b and involves water-mediated proton transfers. From TPS simulations, it was observed that both the proton transfers happen simultaneously, resulting in the formation of a $\rm H_3O^+$ ion. The Gln residue is located quite far from the reaction center (5–6 Å) but holds the water molecule in the optimum position for the reaction to happen because glutamine is a weaker hydrogen bond acceptor compared to glutamic acid.

From a randomly chosen TPS trajectory, it was observed that a water molecule and the Gln26 residue are present roughly at distances of 4 and 7.5 Å from the reaction center, respectively, at the beginning of the trajectory. Gln26 then moves closer (from 7.5 to 5.2 Å), pushing the water molecule in the direction of the oxyanion (O4 atom). Proton transfer from the C8 atom to the water molecule results in the formation of the metastable $\rm H_3O^+$ ion which has a short lifetime of ~20 fs and rapidly donates a proton to the O4 oxyanion. The analysis of the transition states of several trajectories revealed that the hydronium ion is not totally symmetrical, as in the Glu-containing systems. The transition state is described by the average distances $d(\rm OH2-H1) = 1.34 \pm 0.07$ Å, $d(\rm OH2-H2) = 1.00 \pm 0.03$ Å, and $d(\rm OH2-H5) = 1.16 \pm 0.12$ Å.

The free energy profile for this system was calculated as a function of the aforementioned order parameter $\zeta = d(\text{C8-H5}) - d(\text{OH2-H5})$, and the result is shown in Figure 10c. The order parameter for the chosen trajectory spans the range [-2.5 Å, 2.5 Å] for a randomly chosen TPS trajectory, and this was divided into 20 overlapping windows. Within each window, 2300 short TPS trajectories are gathered using the shooting algorithm. The free energy barrier is calculated to be \sim 12 kcal/mol. Experimentally, it was observed that although this mutation reduced the rate of the reaction by a factor of 20 compared to the BH_{MeHis}1.8 variant with the Glu26 residue,

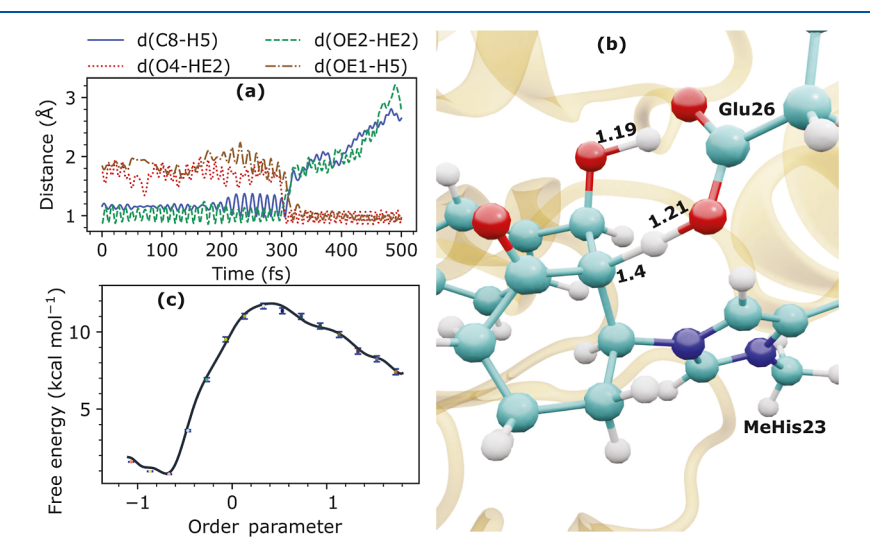


Figure 9. (a) Time series of the evolution of various proton transfer atomic distances along a typical TPS trajectory for the BH_{MeHis}1.8 enzyme with a glutamic acid residue directly responsible for both proton transfers. (b) Geometry of the substrate along with the GluH26 and MeHis23 residues at the transition state calculated using committor analysis for a typical TPS trajectory. (c) Reaction free energy as a function of the order parameter $\zeta = d(C8-H5) - d(OH2-H5)$ calculated using a window-based modified TPS algorithm, where the error bars obtained from bootstrapping analysis are indicated in blue.

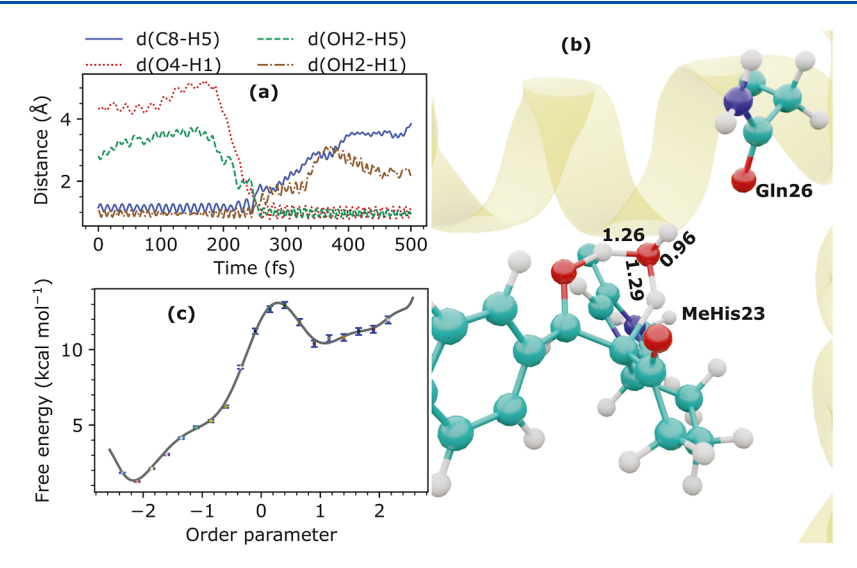


Figure 10. (a) Time series of the evolution of various proton transfer atomic distances along a typical TPS trajectory for the BH_{MeHis}1.8 enzyme with a glutamine residue and water-mediated reaction mechanism. (b) Geometry of the substrate along with the Gln26 and MeHis23 residues at the transition state calculated using committor analysis for a typical TPS trajectory, which indicates the formation of a H_3O^+ ion. (c) Reaction free energy as a function of the order parameter $\zeta = d(C8-H5) - d(OH2-H5)$ calculated using a window-based modified TPS algorithm, where the error bars obtained from bootstrapping analysis are indicated in blue.

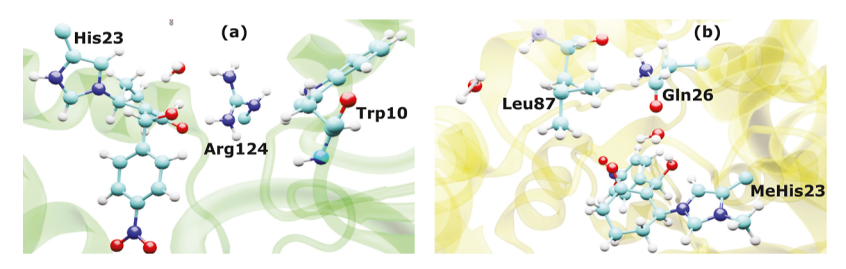


Figure 11. Residues (a) Trp10 in the BH32.12 variant and (b) Leu87 in the $BH_{MeHis}1.8$ variant participating in protein dynamics.

the reaction still proceeded to completion. Our calculations support this observation, since it is evident that the watermediated mechanism is a possible route for the enzyme with the Glu26Gln mutation to complete the reaction. While this system has a free energy barrier comparable to the system with the GluH26 residue, the 20-fold reduction in the rate of the reaction can possibly be explained by the involvement of a water molecule in this reaction. In our calculations, the water molecule is placed where it needs to be, so we might miss an entropic contribution to the free energy barrier. The TPS calculations cannot possibly be made long enough to allow for the inclusion of diffusive water motion. An important question is how we would actually determine the relative importance of mechanisms that involve water or not in the same overall level of protein evolution. One way to begin to tease this experimentally is via solvent isotope effects, and we have suggested such experiments to our collaborators.

Summary of Reaction Kinetics and Protein Dynamics. We found that the two main residues participating in the protein dynamics in the system containing the BH32.12 enzyme are Arg124 and Trp10 (Figure 11a). While Arg124 is stabilizing the oxyanions, as was described in detail in the previous section, Trp10, which is close to the reaction center, assists Arg124 in taking the optimum position in space for hydrogen bond interaction with the substrate. Trp10 can subtly change the orientation of Arg124. For example, the angle (NE1-CD1-NE) between two Trp10 atoms and one Arg124 atom drops by $24 \pm 6^{\circ}$ along the trajectories. As a

result, Arg124 is positioned appropriately to stabilize the oxyanions of the substrate. The substrate, in turn, also undergoes some postreaction changes. The cyclohexanone ring became more planar. The (O3–C13–C12–H11) dihedral decreases by 131 \pm 5°, and its value trends toward zero. The coordinated transfer of the two protons results in an energetically advantageous process. The transfer of both protons has a relatively low free energy barrier of about 10 kcal/mol.

In most cases of MeHis systems, the protein dynamics that can affect the reaction can be described as follows: (i) Glu26 (different protonation states) approaches the reaction center, either pushing a water molecule or directly interacting with the substrate; (ii) the Leu87 residue pushes the Glu26 or changes its plane that may help either initiate the reaction or stabilize the product (Figure 11b). It is worth noting that only in the case of glutamate, Leu87 is located significantly far from Glu26 (>6 Å), and no attempts to approach closer are noticed. The free energy barrier for this system is higher compared to those of the other three systems (Table 1). The strongest interaction between residues Leu87 and Glu26 is observed for the system with glutamic acid in the absence of a water molecule. Before the reaction, the isobutyl group of Leu87 approaches GluH26, forming an H-bond with the OE1 atom. The interatomic distance d(HD22-OE1) between these two residues decreases from 4.30 ± 0.04 to 2.53 ± 0.02 Å and remains small even for some time after the reaction. This indicates that Leu87 pushes GluH26 toward the substrate and can also help stabilize the

Table 1. Free Energy Barriers and Protein Dynamics

system	ΔG^a	protein dynamics
Arg + H ₂ O	10 ± 0.2	Arg124 moves \rightarrow O ⁻ Trp10 interacts with Arg124
Glu + H ₂ O	18 ± 0.4	Glu26 holds the H ₂ O molecule near the reaction center
GluH + H ₂ O	14 ± 0.2	GluH26 moves → reaction center Leu87 interacts with GluH26
GluH	11 ± 0.1	GluH26 moves → reaction center Leu87 interacts with GluH26
Gln + H ₂ O	12 ± 0.2	Gln26 moves \rightarrow reaction center Gln26 pushes the H_2O molecule Leu87 interacts with Gln26

^aThe free-energy value (ΔG) is presented in kcal/mol along with the average standard deviation calculated using bootstrapping analysis.

product. This system has the lowest free energy barrier (Table 1), demonstrating the greatest efficiency of the direct mechanism: no energy is required to move a water molecule to the reaction center, make some kind of intermediate particle, or finally form a product. The product is produced directly after GluH26 interacts with the substrate. The difference between the interaction of Leu87 with GluH26 in the case of the water-mediated GluH26 system is that at the moment of the reaction, the length of the HD22-OE1 bond is not in the range of the H-bond distance (3.69 \pm 0.11 Å). However, after the reaction, it drops to 2.83 ± 0.22 Å, which already corresponds to an H-bond. Thus, Leu87 can also aid in product stabilization. The free energy barrier in this case is slightly higher (14 kcal/mol, Table 1), which can be explained by the presence of a third particle (water molecule). In both of these GluH systems, after protonation of the alkoxide, the negatively charged carboxylate group of Glu26 attracts the isobutyl group of Leu87. The scenario is different in the case of charge-neutral Gln26, where the carboxylic group is substituted by an amine. Prior to the reaction, the d(HD22-OE1) distance between Leu87 and Gln26 increases from 2.28 \pm 0.15 Å to 4.57 ± 0.04 Å. The position of the isobutyl group is changed concurrently. The rotation around the C-C bond can be observed. The CA-CB-CG-CD dihedral reduces by 58 \pm 16°. The Gln's plane is altered by this motion. It may be described by an increase of $82 \pm 23^{\circ}$ in the angle between the CD-OE1 atoms of Gln26 and the CD2 atom of Leu87. All of these rearrangements cause Gln26 to move closer to the reaction center (the distance between Gln26 and the substrate is reduced by 1.95 \pm 0.41 Å) and push a water molecule, thereby initiating the reaction. This demonstrates how pair residues cooperate to provide an energetically favorable mechanism. The barrier of the free energy is 12 kcal/mol (Table 1). In order to design highly active artificial protein catalysts, it is likely that such motions will need to include such aspects of dynamics, again pointing to the great challenge of this program.

CONCLUSIONS

In this manuscript, we theoretically analyzed various reaction mechanisms that are found in artificially evolved enzymes developed by Green and co-workers 16,19 to catalyze a MBH reaction. In particular, we studied the BH32.12 and BH $_{\rm MeHis}$ 1.8 variants which were reported to have high catalytic efficiency and whose crystal structures were readily available. Using TPS simulations, we analyzed the rate-limiting step of this reaction that involves the transfer of two protons between the substrate and the enzyme.

For the BH32.12 variant which consisted of a nucleophilic His23 residue, it was observed from the TPS trajectories that a catalytic Arg124 residue was involved at the reaction center, whereas the transfer of protons was mediated by a water molecule. The proton transfers proceeded in a stepwise manner with the formation of a OH⁻ anion, and the free energy profile consisted of two barriers of magnitudes, 7 and 10 kcal/mol separated by an intermediate state. The second barrier from the intermediate state to the reactant state is only ~2 kcal/mol. We predicted that the reaction catalyzed by the BH32.12 variant would be inefficient because of a combination of the potential entropic cost of the water involvement and competition from the backward reaction (intermediate to reactant).

BH_{MeHis}1.8 had the noncanonical methylhistidine residue as the nucleophile and a catalytic Glu26 residue, which had an unusually large p K_a value. Therefore, we considered three different starting points for the TPS simulations. For two of the cases where the glutamic acid has lost its proton either to the solution or to the substrate and exists as glutamate, it was observed that a water-mediated proton transfer was the only pathway, and for these systems, we calculated free energy barriers of ~20 and ~14 kcal/mol, respectively.

For the third case, when the glutamic acid is intact (GluH26), it was observed to be directly involved in both proton transfers, and a free energy barrier of ~11 kcal/mol was calculated for this system. The three free energy profiles calculated for the possible mechanisms supported by the BH_{MeHis}1.8 variant all had a single barrier, and hence it is theorized that these systems are more efficient than the BH32.12 variant. Furthermore, the third mechanism, which involves the direct proton transfer mediated by the GluH26 residue, avoids the involvement of the catalytic water molecule, has a smaller free energy barrier, and, therefore, is the most efficient variant that we have studied in this work. This is consistent with the proposed reaction mechanisms of Crossley et al. for the $BH_{MeHis}1.8$ enzyme. TPS can be used to observe not only different pathways of complex chemical reactions catalyzed by enzymes but also, by means of transition states, Mulliken charges, and free energy profiles, we are able to distinguish and rank the different pathways based on their efficiency.

Our results also point to the challenges of enzyme design. Because of the obvious centrality of protein dynamics, we see a clear reason why designs based on static structures have little to no activity. Paradigms that include "design for dynamics" that can prebuild needed residue motion introduced by laboratory evolution are a long-term goal. Our previous work shows that alterations of hydrogen bonding patterns are used in the directed evolution optimization that couples protein dynamics to reaction through promoting vibrations, and so that will be the first method used in designing proteins that are dynamically active. 43,44 It should also be noted that quantum tunneling can have large effects on the rates of reaction as well as the kinetic isotope effect (KIE), so the current work is directed at quantum TPS for the proton transfers involved in the MBH reaction.

ASSOCIATED CONTENT

Data Availability Statement

The data corresponding to the free energy calculations of the reactions catalyzed by the BH32.12 and $\rm BH_{MeHis}1.8$ enzymes and python scripts that were used to extract the distributions of

distances from MD trajectories as well as the distributions of order parameters from window-based TPS analysis can be found in the GitHub repository https://github.com/sreeganb/JCIM MBHase-data-scripts.

Supporting Information

The Supporting Information is available free of charge at https://pubs.acs.org/doi/10.1021/acs.jcim.4c00045.

Computational details regarding TPS simulations, committor analysis, and additional free energy calculation results (PDF)

AUTHOR INFORMATION

Corresponding Author

Steven Schwartz — Department of Chemistry and Biochemistry, University of Arizona, Tucson, Arizona 85721, United States; orcid.org/0000-0002-0308-1059; Email: sschwartz@arizona.edu

Authors

Sree Ganesh Balasubramani — Department of Chemistry and Biochemistry, University of Arizona, Tucson, Arizona 85721, United States

Kseniia Korchagina – Department of Chemistry and Biochemistry, University of Arizona, Tucson, Arizona 85721, United States

Complete contact information is available at: https://pubs.acs.org/10.1021/acs.jcim.4c00045

Notes

The authors declare no competing financial interest.

ACKNOWLEDGMENTS

SDS acknowledges funding from the NIH through grant number R35GM45213 and the NSF through grant number MCB-2244981. Dr. Anthony P. Green, Dr. Sam Hay, and Dr. Linus Johannissen are greatly acknowledged for providing the crystal structure for the $\rm BH_{MeHis}1.8$ enzyme and for their insightful comments.

REFERENCES

- (1) Wolfenden, R.; Snider, M. J. The Depth of Chemical Time and the Power of Enzymes as Catalysts. *Acc. Chem. Res.* **2001**, *34*, 938–945.
- (2) Bar-Even, A.; Noor, E.; Savir, Y.; Liebermeister, W.; Davidi, D.; Tawfik, D. S.; Milo, R. The Moderately Efficient Enzyme: Evolutionary and Physicochemical Trends Shaping Enzyme Parameters. *Biochem* **2011**, *50*, 4402–4410.
- (3) Schramm, V. L. Enzymatic transition states and transition state analog design. *Annu. Rev. Biochem.* **1998**, *67*, 693–720.
- (4) Taylor, A. I.; Pinheiro, V. B.; Smola, M. J.; Morgunov, A. S.; Peak-Chew, S.; Cozens, C.; Weeks, K. M.; Herdewijn, P.; Holliger, P. Catalysts from synthetic genetic polymers. *Nature* **2015**, *518*, 427–430
- (5) Kuah, E.; Toh, S.; Yee, J.; Ma, Q.; Gao, Z. Enzyme Mimics: Advances and Applications. *Chem. Eur. J.* **2016**, 22, 8404–8430.
- (6) Jiang, L.; Althoff, E. A.; Clemente, F. R.; Doyle, L.; Röthlisberger, D.; Zanghellini, A.; Gallaher, J. L.; Betker, J. L.; Tanaka, F.; Barbas, C. F.; Hilvert, D.; Houk, K. N.; Stoddard, B. L.; Baker, D. De Novo Computational Design of Retro-Aldol Enzymes. *Science* 2008, 319, 1387–1391.
- (7) Lechner, H.; Ferruz, N.; Höcker, B. Strategies for designing non-natural enzymes and binders. *Curr. Opin. Chem. Biol.* **2018**, 47, 67–76.

- (8) Kiss, G.; Çelebi-Ölçüm, N.; Moretti, R.; Baker, D.; Houk, K. N. Computational Enzyme Design. *Angew. Chem., Int. Ed.* **2013**, *52*, 5700–5725.
- (9) Hossack, E. J.; Hardy, F. J.; Green, A. P. Building Enzymes through Design and Evolution. ACS Catal. 2023, 13, 12436–12444.
- (10) Morita, K.-i.; Suzuki, Z.; Hirose, H. A Tertiary Phosphine-catalyzed Reaction of Acrylic Compounds with Aldehydes. *Bull. Chem. Soc. Jpn.* **1968**, *41*, 2815.
- (11) Basavaiah, D.; Rao, A. J.; Satyanarayana, T. Recent Advances in the Baylis-Hillman Reaction and Applications. *Chem. Rev.* **2003**, *103*, 811–892.
- (12) Wei, Y.; Shi, M. Recent Advances in Organocatalytic Asymmetric Morita-Baylis-Hillman/aza-Morita-Baylis-Hillman Reactions. *Chem. Rev.* **2013**, *113*, 6659–6690.
- (13) Shi, M.; Liu, X.-G. Asymmetric Morita-Baylis-Hillman Reaction of Arylaldehydes with 2-Cyclohexen-1-one Catalyzed by Chiral Bis(Thio)urea and DABCO. *Org. Lett.* **2008**, *10*, 1043–1046.
- (14) Barbier, V.; Couty, F.; David, O. R. P. Morita—Baylis—Hillman Reactions with Nitroalkenes: A Case Study. *Eur. J. Org Chem.* **2015**, 2015, 3679—3688.
- (15) Aggarwal, V. K.; Mereu, A. Superior amine catalysts for the Baylis—Hillman reaction: the use of DBU and its implications. *Chem. Commun.* 1999, 2311–2312.
- (16) Crawshaw, R.; Crossley, A. E.; Johannissen, L.; Burke, A. J.; Hay, S.; Levy, C.; Baker, D.; Lovelock, S. L.; Green, A. P. Engineering an efficient and enantioselective enzyme for the Morita-Baylis-Hillman reaction. *Nat. Chem.* **2022**, *14*, 313–320.
- (17) Bjelic, S.; Nivón, L. G.; Çelebi-Ölçüm, N.; Kiss, G.; Rosewall, C. F.; Lovick, H. M.; Ingalls, E. L.; Gallaher, J. L.; Seetharaman, J.; Lew, S.; Montelione, G. T.; Hunt, J. F.; Michael, F. E.; Houk, K. N.; Baker, D. Computational Design of Enone-Binding Proteins with Catalytic Activity for the Morita-Baylis-Hillman Reaction. *ACS Chem. Biol.* **2013**, *8*, 749–757.
- (18) Alford, R. F.; Leaver-Fay, A.; Jeliazkov, J. R.; O'Meara, M. J.; DiMaio, F. P.; Park, H.; Shapovalov, M. V.; Renfrew, P. D.; Mulligan, V. K.; Kappel, K.; Labonte, J. W.; et al. The Rosetta All-Atom Energy Function for Macromolecular Modeling and Design. *J. Chem. Theory Comput.* **2017**, *13*, 3031–3048.
- (19) Crossley, A. E.; Crawshaw, R.; Hardy, F. J.; Johannissen, L.; Lister, T. M. F. G. E.; Birch-Price, Z.; Obexer, R.; Hay, S.; Green, A. P. A non-canonical nucleophile unlocks a new mechanistic pathway in a designed enzyme. *Nat. Chem. Biol.* **2023**, *100* (21), 12129–12134.
- (20) Bolhuis, P. G.; Chandler, D.; Dellago, C.; Geissler, P. L. Transition Path Sampling: Throwing Ropes Over Rough Mountain Passes, in the Dark. *Annu. Rev. Phys. Chem.* **2002**, *53*, 291–318.
- (21) Dellago, C.; Bolhuis, P. G. Advanced Computer Simulation Approaches for Soft Matter Sciences III, 2009, pp 167-233.
- (22) Basner, J. E.; Schwartz, S. D. How Enzyme Dynamics Helps Catalyze a Reaction in Atomic Detail: A Transition Path Sampling Study. *J. Am. Chem. Soc.* **2005**, *127*, 13822–13831.
- (23) Schramm, V. L.; Schwartz, S. D. Promoting Vibrations and the Function of Enzymes. Emerging Theoretical and Experimental Convergence. *Biochem* **2018**, *57*, 3299–3308.
- (24) Schwartz, S. D.; Schramm, V. L. Enzymatic transition states and dynamic motion in barrier crossing. *Nat. Chem. Biol.* **2009**, *5*, 551–558.
- (25) Radhakrishnan, R.; Schlick, T. Biomolecular free energy profiles by a shooting/umbrella sampling protocol, "BOLAS. *J. Chem. Phys.* **2004**, *121*, 2436–2444.
- (26) Masterson, J. E.; Schwartz, S. D. Changes in Protein Architecture and Subpicosecond Protein Dynamics Impact the Reaction Catalyzed by Lactate Dehydrogenase. *J. Phys. Chem. A* **2013**, *117*, 7107–7113.
- (27) Senn, H. M.; Thiel, W. QM/MM Methods for Biomolecular Systems. *Angew. Chem., Int. Ed.* **2009**, *48*, 1198–1229.
- (28) Field, M. J.; Bash, P. A.; Karplus, M. A combined quantum mechanical and molecular mechanical potential for molecular dynamics simulations. *J. Comput. Chem.* **1990**, *11*, 700–733.

- (29) Vanommeslaeghe, K.; Hatcher, E.; Acharya, C.; Kundu, S.; Zhong, S.; Shim, J.; Darian, E.; Guvench, O.; Lopes, P.; Vorobyov, I.; Mackerell, A. D. CHARMM general force field: A force field for druglike molecules compatible with the CHARMM all-atom additive biological force fields. *J. Comput. Chem.* **2010**, *31*, 671–690.
- (30) Repasky, M. P.; Chandrasekhar, J.; Jorgensen, W. L. PDDG/PM3 and PDDG/MNDO: Improved semiempirical methods. *J. Comput. Chem.* **2002**, 23, 1601–1622.
- (31) Gao, J.; Amara, P.; Alhambra, C.; Field, M. J. A Generalized Hybrid Orbital (GHO) Method for the Treatment of Boundary Atoms in Combined QM/MM Calculations. *J. Phys. Chem. A* **1998**, 102, 4714–4721.
- (32) Jorgensen, W. L.; Chandrasekhar, J.; Madura, J. D.; Impey, R. W.; Klein, M. L. Comparison of simple potential functions for simulating liquid water. *J. Chem. Phys.* **1983**, *79*, 926–935.
- (33) Ryckaert, J.-P.; Ciccotti, G.; Berendsen, H. J. Numerical integration of the cartesian equations of motion of a system with constraints: molecular dynamics of n-alkanes. *J. Comput. Phys.* **1977**, 23, 327–341.
- (34) Brooks, B. R.; Brooks, C. L.; Mackerell, A. D.; Nilsson, L.; Petrella, R. J.; Roux, B.; Won, Y.; Archontis, G.; Bartels, C.; Boresch, S.; Caflisch, A.; Caves, L.; et al. CHARMM: The biomolecular simulation program. *J. Comput. Chem.* **2009**, *30*, 1545–1614.
- (35) Bolhuis, P. G.; Dellago, C. Practical and conceptual path sampling issues. *Eur. Phys. J.: Spec. Top.* **2015**, 224, 2409–2427.
- (36) Bolhuis, P. G.; Swenson, D. W. H. Transition Path Sampling as Markov Chain Monte Carlo of Trajectories: Recent Algorithms, Software, Applications, and Future Outlook. *Adv. Theory Simul.* **2021**, 4, 2000237.
- (37) Dellago, C.; Bolhuis, P. G.; Geissler, P. L. Advances in Chemical Physics; John Wiley & Sons, Ltd, 2002; Chapter 1, pp 1–78.
- (38) Brotzakis, Z. F.; Bolhuis, P. G. A one-way shooting algorithm for transition path sampling of asymmetric barriers. *J. Chem. Phys.* **2016**, *145*, 164112.
- (39) Bolhuis, P. G.; Dellago, C.; Chandler, D. Reaction coordinates of biomolecular isomerization. *Proc. Natl. Acad. Sci. U.S.A.* **2000**, *97*, 5877–5882.
- (40) Geissler, P. L.; Dellago, C.; Chandler, D. Kinetic Pathways of Ion Pair Dissociation in Water. *J. Phys. Chem. B* **1999**, *103*, 3706–3710.
- (41) Antoniou, D.; Schwartz, S. D. The stochastic separatrix and the reaction coordinate for complex systems. *J. Chem. Phys.* **2009**, *130*, 151103.
- (42) Balasubramani, S. G.; Schwartz, S. D. Transition Path Sampling Based Calculations of Free Energies for Enzymatic Reactions: The Case of Human Methionine Adenosyl Transferase and Plasmodium vivax Adenosine Deaminase. *J. Phys. Chem. B* **2022**, *126*, 5413–5420.
- (43) Schafer, J. W.; Zoi, I.; Antoniou, D.; Schwartz, S. D. Optimization of the Turnover in Artificial Enzymes via Directed Evolution Results in the Coupling of Protein Dynamics to Chemistry. *J. Am. Chem. Soc.* **2019**, *141*, 10431–10439.
- (44) Schafer, J. W.; Schwartz, S. D. Directed Evolution's Influence on Rapid Density Fluctuations Illustrates How Protein Dynamics Can Become Coupled to Chemistry. *ACS Catal.* **2020**, *10*, 8476–8484.
- (45) Bolhuis, P. G. Transition-path sampling of β -hairpin folding. *Proc. Natl. Acad. Sci. U.S.A.* **2003**, *100*, 12129–12134.